MCB
Journals.ASM.org

Caspase-3 Protects Stressed Organs against Cell Death

Hadi Khalil,[a] Nieves Peltzer,[a] Joël Walicki,[a] Jiang-Yan Yang,[a] Gilles Dubuis,[a] Noémie Gardiol,[b] Werner Held,[b] Paul Bigliardi,[c]* Benjamin Marsland,[d] Lucas Liaudet,[e] and Christian Widmann[a]

Department of Physiology[a] and Ludwig Center for Cancer Research of the University of Lausanne,[b] Faculty of Biology and Medicine, University of Lausanne, Lausanne, Switzerland, and Department of Dermatology,[c] Department of Pneumology,[d] and Department of Intensive Care Medicine,[e] Centre Hospitalier Universitaire Vaudois and University of Lausanne, Lausanne, Switzerland

The ability to generate appropriate defense responses is crucial for the survival of an organism exposed to pathogenesis-inducing insults. However, the mechanisms that allow tissues and organs to cope with such stresses are poorly understood. Here we show that caspase-3-knockout mice or caspase inhibitor-treated mice were defective in activating the antiapoptotic Akt kinase in response to various chemical and environmental stresses causing sunburns, cardiomyopathy, or colitis. Defective Akt activation in caspase-3-knockout mice was accompanied by increased cell death and impaired survival in some cases. Mice homozygous for a mutation in RasGAP that prevents its cleavage by caspase-3 exhibited a similar defect in Akt activation, leading to increased apoptosis in stressed organs, marked deterioration of their physiological functions, and stronger disease development. Our results provide evidence for the relevance of caspase-3 as a stress intensity sensor that controls cell fate by either initiating a RasGAP cleavage-dependent cell resistance program or a cell suicide response.

Executioner caspases mediate cell death during apoptosis (45). Of these, caspase-3 has the ability to cleave the majority of the caspase substrates (43), and its activity is required for the induction of cell death in response to many apoptotic stimuli (1). While executioner caspases are indispensable for apoptosis, there are situations when their activation does not lead to death. For example, healthy dividing cells can weakly activate caspase-3 in response to mild stresses (47). Caspase-3 also participates, in an apoptosis-independent manner, in T and B cell homeostasis (35, 46), in microglia activation (6), in long-term depression (26), and in muscle (17), monocyte (44), embryonic stem cell (18), and erythroid cell (13) differentiation. However, it remains unclear how activation of caspase-3 under these conditions does not eventually lead to cell death (1, 24). Cells could have an intrinsic ability to tolerate low caspase activity by constitutively expressing antiapoptotic molecules, such as members of the inhibitors of the apoptosis protein family, or may stimulate antiapoptotic pathways in parallel to caspase activation (24). Alternatively, the caspases themselves might activate prosurvival pathways, in particular, when they are mildly stimulated. Indeed, there is evidence in cultured cells that caspase-3 mediates neuroprotection after preconditioning (30) and that caspase-3 activity turns on the antiapoptotic Akt kinase following partial cleavage of the RasGAP protein (47). Other caspase substrates that could potentially induce protective signals once cleaved include $p27^{kip1}$ (14), Lyn (28), synphilin-1 (19), and Rb (42), yet the physiological importance of these cleaved substrates has not been evaluated to date.

In the present study, we have investigated the role played by caspase-3 and its substrate p120 RasGAP in the induction of the antiapoptotic Akt kinase in stressed tissues *in vivo*.

MATERIALS AND METHODS

Caspase-3-KO mice. B6.129S1-*Casp3*^{tm1Flv}/J caspase-3-knockout (KO) mice were purchased from the Jackson Laboratory (Bar Harbor, ME). The mice were genotyped using a mixture of the following three oligonucleotides: wild-type sense (GCG AGT GAG AAT GTG CAT AAA TTC), wild-type antisense (GGG AAA CCA ACA GTA GTC AGT CCT), and caspase-3-knockout antisense (TGC TAA AGC GCA TGC TCC AGA CTG). The sizes of the amplified fragments are 320 bp for the wild-type allele and 300 bp for the caspase-3-knockout allele.

Generation of RasGAP D455A-knock-in (KI) mice. The strategy and methods used to create the targeting vector are presented in Fig. S1 in the supplemental material.

UV-B exposure and isolation of skin samples. Mice were shaved on both flanks, followed by depilation with depilatory cream (Veet), and 48 h later were anesthetized and illuminated with a Waldmann UV801 KL apparatus equipped with a Philips UV21 UV-B lamp (TL 20W/12RS). The doses of UV-B illumination were 0.05 and 0.3 J/cm^2 (i.e., 50 mJ/cm^2 and 300 mJ/cm^2, respectively), which were measured with a Waldmann Variocontrol dosimeter. In each case, only one side of the mouse was illuminated and the other side was used as a control (i.e., nonexposed skin). Mice were sacrificed 24 h after illumination. The lateral skin biopsy specimens (approximately 2 by 2 cm) were excised from each mouse, fixed in phosphate-buffered saline (PBS) and 4% Formol solution, and embedded in paraffin. The paraffin-embedded skin was cut into 4-μm sections, deparaffinized, and stained with hematoxylin-eosin for histological observation.

Doxorubicin injection and hemodynamic measurements using left ventricular PV microcatheters. Eight-week-old mice were weighed and injected with a single intraperitoneal doxorubicin dose of 20 mg/kg of body weight using a 2-mg/ml doxorubicin solution (catalog number 733857-01; EBEWE Pharma) or injected with an equal volume of saline (catalog number 534534; B. Braun Medical AG). At 5 days postinjection, the animals were weighed again (the weight loss at that time was between 10 and 15%). The animals were anesthetized with an intraperitoneal in-

Received 8 June 2012 Returned for modification 9 July 2012
Accepted 29 August 2012
Published ahead of print 4 September 2012
Address correspondence to Christian Widmann, Christian.Widmann@unil.ch.
* Present address: Paul Bigliardi, NUHS/NUS and IMB/A*STAR, Singapore, Singapore.
H.K. and N.P. contributed equally to this article.
Supplemental material for this article may be found at http://mcb.asm.org/.

doi:10.1128/MCB.00774-12

jection of 75 mg/kg ketamine and 10 mg/kg xylazine (the volume of injection was 10 μl per g of mouse). A pressure-volume (PV) SPR-839 catheter (Millar Instruments, Houston, TX) was inserted into the left ventricle (LV) via the right carotid artery. After stabilization for 20 min, heart rate, LV systolic and end-diastolic pressures, and volumes were measured, and stroke volume, ejection fraction, and cardiac output were calculated and corrected according to *in vitro* and *in vivo* volume calibrations with a cardiac PV analysis program (PVAN3.2; Millar Instruments) (38, 39). End-systolic LV PV relationships were assessed by transiently reducing venous return by compressing the inferior vena cava, and LV contractility was assessed from the slope of the LV end-systolic PV relationship (end-systolic elastance), calculated using PVAN3.2, as detailed previously (21, 38). Hearts were isolated, cut into two pieces, and then either snap-frozen or fixed in 4% formalin for histology studies.

DSS-induced colitis and clinical score. Eight-week-old mice were given acidified water supplemented with 5% (wt/vol) dextran sodium sulfate (DSS; molecular weight, 400,000 to 600,000; MP Biomedicals, Illkirch, France) for 72 h and then given normal drinking water for four additional days. Mice were examined daily, and body weight, water consumption, occult blood, and diarrhea were measured. At day 7, mice were sacrificed, the colon length was measured, and a clinical score was estimated according to the procedure described by Ohkawara et al. (36). Percentage of weight loss was calculated by comparing the weight at day 0 and the weight of the mice at sacrifice. Scores were given according to the extent of weight loss: 0, no weight loss; 1, 1 to 5%; 2, 5 to 10%; 3, 10 to 15%; 4, >15%. Diarrhea was scored using a scale with values ranging from 0 to 4: 0, normal; 1, slightly loose feces; 2, loose feces; 3, semiliquid stool; and 4, liquid stool. Fecal occult blood was detected using guaiac paper (ColoScreen Hemocult kit; Helena Labs, Beaumont, TX), and the associated scores were as follows: 0, none; 2, positive Hemocult result; and 4, gross bleeding. Colons were cut into three equal portions (proximal, middle, and distal), and each portion was further cut into three equal parts, two of which were snap-frozen in liquid N_2 and stored at −80°C for subsequent protein and RNA analysis, and the third portion was fixed in 4% formalin for histology analysis (paraffin sections).

Quantitation of active Akt- and active caspase-3-positive cells in heart, skin, and colon. Sections stained as described in the previous sections were scanned using an automated Nikon Eclipse 90i microscope equipped with Apo Plan ×20 (0.75 pH 2 PM) and Apo Plan ×40/1.0 DIC-H objectives and piloted with NIS-Elements Advance Research software (Nikon Instruments Inc., Melville, NY).

Three whole-heart sections were scanned at different levels, and the corresponding whole-section images were generated. The number of pAkt-positive cells was scored manually by counting the number of cells stained with the anti-phospho-Akt antibody (the samples were randomized prior to examination, and the person performing the counting was not aware of the experimental conditions). The total number of cells was determined by automatically scoring the number of nuclei (stained with the Hoechst 33342 dye) using the NIS-Elements AR program (Nikon). In order to minimize errors, all images were acquired with the same contrast (high), size and quality (1280 × 960 pixels), exposure time (4′,6-diamidino-2-phenylindole [DAPI], 40 ms; fluorescein isothiocyanate [FITC], 300 ms), and gain (1×). The quantification threshold in the automated measurement menu was set at L32 for low and H236 for high, and the area was restricted to 0 to 0.5 μm^2 out. In the image menu, the local contrast was set to 30, and in the image-background option, the background was set to 40 for DAPI and to 999 for FITC. Using the binary menu, the holes were filled using the fill holes option. This was performed to avoid multiple counting of the same nucleus. Touching nuclei were separated using the morpho separate objects option. The number of nuclei was displayed under automated measurement results—object data. Skin sections were scanned and analyzed similarly. Fifteen different fields were randomly taken from the proximal, middle, and distal sections of the colon and processed and analyzed as described above.

Apoptosis scoring. Apoptosis on histological slides was assessed by terminal deoxynucleotidyltransferase-mediated dUTP-biotin nick end labeling (TUNEL) assay (DeadEnd Fluorometric TUNEL system; catalog number G3250; Promega Switzerland), as per the manufacturer's protocol, and quantitated as described for the Akt staining in the previous section. Apoptosis *in vitro* counting was assessed by scoring the number of cells with pycnotic or fragmented nuclei after Hoechst 33342 staining (48).

Chemicals and antibodies. The quinolyl-valyl-*O*-methylaspartyl-[2,6-difluorophenoxy]-methyl ketone (Q-VD-OPh) caspase inhibitor was from MP Biomedicals (catalog number OPH109). Hexameric FasL (fusion protein between the Fas ligand and the Fc portion of IgG1) (20) was a kind gift from Pascal Schneider (University of Lausanne). The monoclonal and polyclonal anti-phospho-Ser473 Akt antibodies and the cleaved caspase-3-specific antibody were from Cell Signaling Technology (catalog numbers 4051, 9271, and 9664, respectively). The monoclonal anti-phospho-Ser^{473} Akt antibody was used on skin and colon sections as well as for Western blot assays, while the polyclonal anti-phospho-Ser^{473} Akt antibody was used on heart sections. The antibody recognizing total Akt was from Santa Cruz (catalog number sc-8312). The anti-RasGAP antibody was from Enzo Life Science (catalog number ALX-210-860-R100). Secondary antibodies (Cy3-coupled donkey anti-rabbit, horseradish peroxidase [HRP]-coupled donkey anti-rabbit, and HRP-coupled donkey anti-mouse antibodies) were from Jackson Immunoresearch (catalog numbers 711-165-152, 715-035-152, and 715-035-150, respectively).

Protein extraction. Snap-frozen skin (0.3-cm^2 biopsy specimens), heart, and intestine tissue samples were crushed into powder in liquid nitrogen-dipped mortar and pestle and then suspended in 700 μl lysis buffer (Tris-HCl, 50 mM; EDTA, 1 mM; EGTA, 1 mM; Triton X-100, 1%; dithiothreitol, 1 mM; sodium pyrophosphate, 5 mM; NaF, 50 mM; protease inhibitor cocktail tablet [1 tablet/40 ml buffer; catalog number 04 693 132 001; Roche]; phenylmethylsulfonyl fluoride, 1 mM; glycerol, 10%; pH 7.4). The samples were sonicated (amplitude, 80%; 5 s; twice). Protein concentration was measured by the Bradford assay using bovine serum albumin (BSA) as a standard. Lysates were mixed with an equal volume of 2× sample buffer (100 mM Tris-HCl [pH 6.8], 20% glycerol, 10% [vol/vol] β-mercaptoethanol, 4% [wt/vol] sodium dodecyl sulfate [SDS], and 0.02% bromophenol blue) and boiled for 5 min at 95°C before loading on SDS-polyacrylamide gels.

Western blotting. Western blotting was performed and quantitated as described previously (31).

Preparation of tissue section and immunohistochemistry. Mice were euthanized by cervical dislocation. The isolated organs (heart, skin, or intestine) were stored in PBS–4% Formol solution and embedded in paraffin. Four-micrometer sections were deparaffinized in toluene (catalog number 488555; Carlo Erba, Milan, Italy) and rehydrated using graded alcohol and distilled water. Antigen retrieval was performed by immersing sections in sodium citrate buffer (10 mM sodium citrate, pH 6), followed by heating in a microwave oven for 20 min (8 min at 800 W and 12 min at 400 W). Sections were cooled to room temperature and blocked using a 50 mM Tris-HCl, pH 7.6, 0.5% Tween 20, 0.2% BSA solution. The primary antibody was diluted (pAkt, 1/100; cleaved caspase-3, 1/200) in 50 mM Tris-HCl, pH 7.6, 0.5% Tween 20, 0.2% BSA and incubated with the slides for 1 h. Slides were washed 2 times for 10 min each time in 50 mM Tris-HCl, pH 7.6, 0.5% Tween 20. The fluorochrome-conjugated secondary antibody (Jackson Laboratory), diluted 1:300 in 50 mM Tris-HCl, pH 7.6, 0.5% Tween 20, 0.2% BSA, was incubated with the slides for another hour in the dark. Slides were then extensively washed (at least 6 times with one overnight washing step). The nuclei in the sections were then stained with 10 μg/ml Hoechst 33342. Finally, the slides were mounted in Mowiol (catalogue number 81381; Fluka) at a concentration of 0.1 mg/ml in a solution made of 20% glycerol and 0.1% DABCO (diazobiciclo-octane; catalogue number 33480; Fluka).

Immunohistochemistry with tyramide signal amplification. Tyramide amplification of immunohistochemical signals using phospho-Akt-

specific antibodies was performed as described earlier (4). The primary antibody and the secondary HRP-coupled antibody were diluted 1/100 and 1/1,000, respectively.

Ethics statement. Experiments on the mice were carried out in strict accordance with the Swiss Animal Protection Ordinance (OPAn). The protocol was approved by the Veterinary Office of the state of Vaud, Switzerland (permit numbers 2055, 2056, and 2361).

MEF preparation. Mouse embryonic fibroblasts (MEFs) from KI and wild-type mice were initially prepared as described earlier by digesting embryonic day 14 embryos for 1.5 h in 0.05% trypsin (5). Using this protocol, MEFs could be generated from wild-type embryos, but none were obtained from the KI embryos (Fig. 5C). Reducing the incubation time in trypsin to 15 min, which presumably lessened a stressful situation on cells, however, allowed production of both wild-type and KI MEFs in more or less similar numbers (Fig. 5C).

Statistics. SAS/STAT (version 9.1) software (SAS Institute Inc., Cary, NC) was used to perform the statistical analyses. Unless otherwise stated, one-way analyses of variance were performed to determine the significance of the observed differences presented in the figures. Asterisks and NS in the figures indicate significant differences ($P < 0.05$) and no significant differences, respectively.

RESULTS

Mice lacking caspase-3 are impaired in their capacity to activate Akt in response to stress. Akt (also called PKB) is a downstream effector of phosphatidylinositol 3-kinase (PI3K) that mediates the survival responses of many cell types and tissues (40) and as such could be involved in stress survival responses across most, if not all, tissues. To determine whether Akt is activated in various tissues and organs in response to pathology-inducing stresses, mice were exposed to three different challenges: exposure of the skin to UV-B, injection of doxorubicin (an anticancer drug inducing cardiomyopathy), and administration of dextran sodium sulfate (DSS) via drinking water to induce colitis. In control skin, very few keratinocytes (~0.25%) expressed the active phosphorylated form of Akt (Fig. 1A). In response to mild UV-B exposure (0.05 J/cm^2), more than 10% of the keratinocytes had active Akt in their cytoplasm (Fig. 1A). In the hearts of untreated mice, cells expressing activated Akt were readily observed. Virtually all of these cells were cardiomyocytes, as determined by their shape and nucleus location (Fig. 1B). Under basal conditions (i.e., no treatment), the percentage of cells with active Akt was much higher in the heart (~6%) than in the epidermis. Doxorubicin increased the percentage of Akt-positive cardiomyocytes in a statistically significant manner to ~10% (Fig. 1B, gray bars). Akin to the situation encountered in the skin, very few cells in the colon epithelium (~0.7%) were found to be positive for active Akt (Fig. 1C). This percentage significantly increased to ~1.2% when colitis was induced by DSS (Fig. 1C, gray bars).

To determine whether Akt activation was dependent on caspase-3, we analyzed caspase-3-KO mice on the C57BL6 background . In this background, caspase-3-KO mice reach adulthood and breed (25). When the skin of these mice was exposed to UV-B, the number of keratinocytes with active Akt increased (Fig. 1A, lower right), suggesting that a caspase-3-independent mechanism can participate in the induction of protective signals in the epidermis. However, the UV-B-induced increase in the percentage of active Akt-positive keratinocytes in caspase-3-KO mice was much reduced compared to the situation observed in wild-type mice, and the increase was not statistically significant (Fig. 1A, black bars). This indicates that caspase-3 is required for a maximal Akt response in keratinocytes subjected to UV-B illumination. When

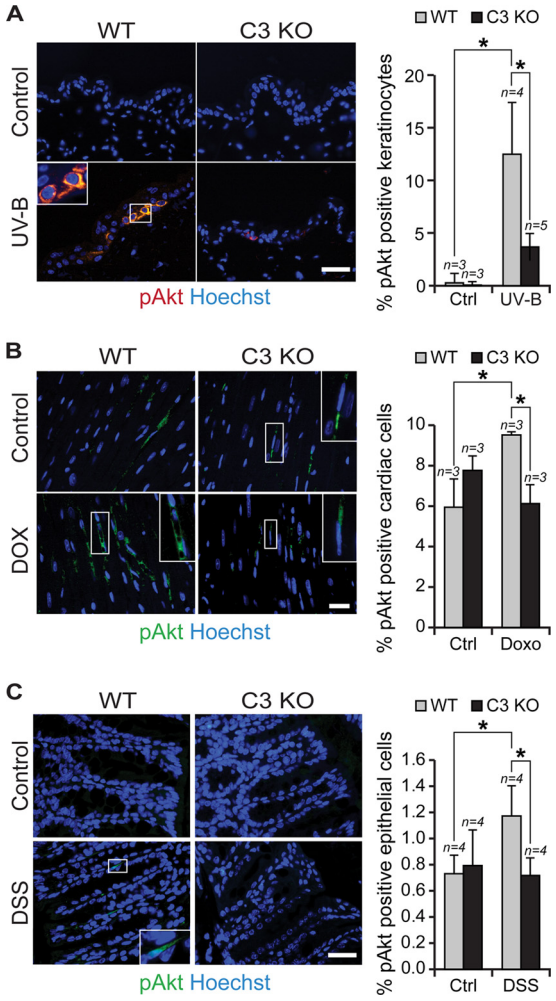

FIG 1 Defective stress-induced Akt activation in mice lacking caspase-3. The indicated numbers of wild-type (WT) and caspase-3-knockout (C3 KO) mice were subjected or not subjected to illumination of their skin with 0.05 J/cm^2 UV-B (A; 2 independent experiments), injection of 20 mg/kg doxorubicin (DOX or Doxo) (B; 2 independent experiments), or exposure to 5% DSS in the drinking water (C; 3 independent experiments) (see Materials and Methods for details). (A to C) Histological sections of the organs and tissues targeted by these stresses were then stained with an antibody recognizing the active phosphorylated form of Akt, and the percentage of phospho-Akt (pAkt)-positive cells was quantitated. Results correspond to the mean ± 95% CI. The images shown are representative examples of sections labeled with the anti-phospho-Akt antibody (red or green staining) and with Hoechst 33342 (blue staining of the nuclei). Bars, 20 μm.

caspase-3-KO mice were treated with doxorubicin or DSS, the percentage of cells with active Akt in the targeted organs did not change compared to the nonchallenged situation (compare the gray and black bars in Fig. 1B and C), indicating that caspase-3 is strictly required for Akt activation in these tissues exposed to stress. To determine if stimulation of caspase-3 activity and not some other noncatalytic functions of the protease is necessary for stress-induced Akt activation, wild-type mice were injected with Q-VD-OPh, a broad-spectrum caspase inhibitor (10). Figures 2A and B show that this compound inhibited UV-B-induced caspase-3 activation in the skin. Q-VD-OPh was found to significantly decrease the ability of epidermal cells to stimulate Akt in response to UV-B (Fig. 2C), indicating that activation of caspases

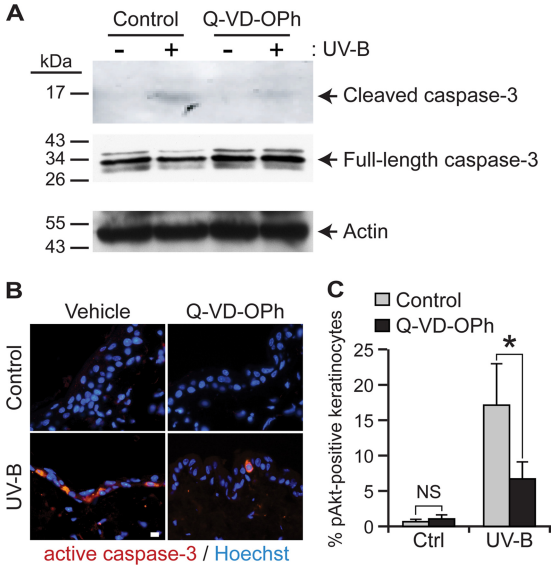

FIG 2 Pharmacological inhibition of caspases hampers UV-B-induced Akt activation in the epidermis. Wild-type mice were injected or not with 50 mg of the Q-VD-OPh caspase inhibitor per kg of mouse 15 min prior to UV-B exposure of the skin (0.3 J/cm^2 [A and B] and 0.05 J/cm^2 [C]). (A) Levels of cleaved active caspase-3, full-length inactive caspase-3, and actin were assessed by Western blotting. This experiment was repeated once with similar results. (B) Levels of active caspase-3 *in situ* were also visualized by immunofluorescence. Bar, 20 μm. The pictures are representative images of data obtained with three mice per condition. (C) Levels of phosphorylated Akt were assessed as described in Fig. 1. Results correspond to the mean ± 95% CI of 3 independent experiments ($n = 3$).

is required for the induction of the antiapoptotic Akt kinase in response to stress.

Increased stress-induced cell death and cell damage in mice lacking caspase-3. Impaired Akt activation in caspase-3-knockout mice may not lead to visible damage of the targeted tissues if the absence of caspase-3 prevents implementation of a cell death response. There are indeed situations where caspase-3 is mandatory for cell death. For example, beta cells from caspase-3-KO mice are fully resistant against streptozotocin-induced death, while beta cells from wild-type mice are not, leading to the development of diabetes (27). In other situations, cell death may still occur in the absence of caspase-3, either as a result of a nonapoptotic type of death or because apoptosis is mediated by other executioner caspases (e.g., caspase-7). In such cases, the absence of a caspase-3-mediated Akt activation might have detrimental consequences. To assess this point, we monitored the extent of stress-induced cell death in the skin and the heart of caspase-3-KO and wild-type mice.

In the skin of wild-type mice, UV-B induced the appearance of keratinocytes with a pycnotic nucleus and densely staining glassy cytoplasm—the so-called sunburn cells (see the inset in the lower left-hand panel in Fig. 3A)—which are apoptotic cells characteristic of those in damaged skin following UV exposure (12). The percentage of sunburn cells generated by UV-B in the skin of caspase-3-KO mice was significantly reduced compared to that in the skin of wild-type mice (Fig. 3A). Similarly, there were fewer TUNEL-positive keratinocytes in the UV-B-illuminated skin of caspase-3-KO mice than in the skin of wild-type mice (Fig. 3B). This indicates that caspase-3 is a main mediator of UV-B-induced keratinocyte apoptosis. Cells can also die in a necrosis-like, nonapoptotic manner, in particular, when apoptosis pathways are altered (41). Keratinocytes dying in this way are characterized by their irregular shape, an eosinophilic cytoplasm, and hyperchromatic, condensed, and partly fragmented nuclei (3) (see the inset in the lower right-hand panel in Fig. 3A). UV-B dramatically increased the percentage of keratinocytes undergoing this type of death in the skin of caspase-3-KO mice compared to the skin of wild-type mice (Fig. 3A). When accounting for both apoptosis and necrosis-like deaths, there was more UV-B-mediated death recorded in the skin of caspase-3-KO mice than in the skin of wild-type mice (8.1% ± 2.5% versus 4.9% ± 1.2%; mean ± 95% confidence interval [CI]).

Doxorubicin is a DNA-intercalating drug that induces both caspase-dependent and -independent cell death in various cell types (29), including cardiomyocytes (51). In response to doxorubicin injection, the percentage of cardiomyocytes undergoing apoptosis, as assessed with the TUNEL assay (see a representative example on the left-hand side of Fig. 3C), was significantly higher in caspase-3-KO mice than wild-type mice (Fig. 3C). It therefore appears that apoptosis induced by doxorubicin can be mediated by executioner caspases other than caspase-3, which is consistent with the observation that doxorubicin efficiently activates caspase-7 (11).

The increased susceptibility of caspase-3-KO mice to doxorubicin-induced cardiomyocyte apoptosis raised the possibility that the lack of caspase-3 affects survival of mice treated with doxorubicin. Figure 3D shows that caspase-3-KO mice survived doxorubicin treatment less efficiently than wild-type mice. This suggests that caspase-3 mediates a protective response in doxorubicin-treated animals that is required to counteract tissue damage induced in a caspase-3-independent manner.

In conclusion, the results presented in Fig. 1 to 3 show that, upon stress exposure, mice lacking caspase-3 are defective in the activation of the prosurvival Akt kinase and that this correlates with increased cell death, tissue damage, and even death of the animals.

Generation of mice expressing a caspase-3-resistant RasGAP mutant. *In vitro*, low caspase-3 activity leads to the cleavage of the p120 RasGAP protein into an amino-terminal fragment, called fragment N, that stimulates Akt in a Ras/PI3K-dependent manner (47, 50), preventing further caspase-3 activation and apoptosis (47). In the presence of high caspase-3 activity, fragment N is further cleaved into two additional fragments (fragments N1 and N2) that are unable to activate Akt (48). Notably, this second cleavage event does not take place if the first cleavage is prevented (49). Further, in the absence of caspase-3 in cells, other executioner caspases, such as caspase-6 and caspase-7, cannot cleave RasGAP (47). RasGAP is therefore a specific caspase-3 substrate. To assess the role of fragment N in Akt stimulation in stressed organs, we generated a KI mouse in which the first RasGAP cleavage site recognized by caspase-3 was destroyed by an aspartate-to-alanine substitution at position 455 (DTVA[455]G) (Fig. 4A and B); the construction of the targeting vector is shown in Fig. S1 in the supplemental material, and genetic analyses of the resulting mice are shown in Fig. 4B and C. This mutation does not affect the function of full-length RasGAP (47). Mice homozygous for the RasGAP^{D455A} allele (KI mice) are viable and fertile, grow normally (Fig. 4D), and show no obvious morphological alterations (Fig. 4E), histologic defects (data not shown), or hematologic abnor-

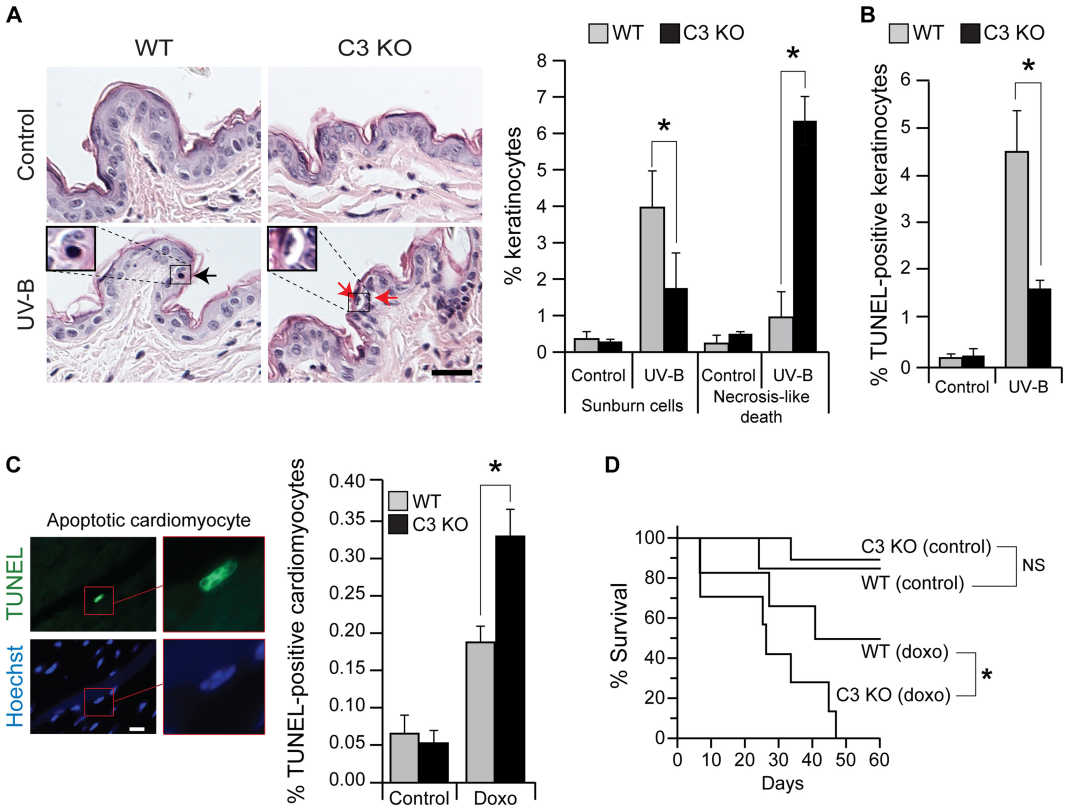

FIG 3 Increased stress-induced cell death and cell damage in mice lacking caspase-3. (A) Histological assessment of sunburn (black arrow) and necrotic-like (red arrows) cells in the epidermis (left and middle) of UV-B (0.05-J/cm^2)-irradiated mouse skin. Results correspond to the mean ± 95% CI of measurements performed on 3 and 8 control and irradiated animals, respectively. Bar, 20 μm. (B) Quantitation of TUNEL-positive keratinocytes following UV-B (0.05-J/cm^2) irradiation. Results correspond to the mean ± 95% CI (3 animals per condition). (C) Apoptosis assessment by the TUNEL assay in cardiomyocytes from mice injected with 20 mg/kg doxorubicin 5 days earlier. A representative example of an apoptotic cardiomyocyte is shown on the left. Bar, 10 μm. Results correspond to the mean ± 95% CI (3 animals per condition). (D) Survival curves of 6 wild-type and 7 caspase-3-KO mice injected with 20 mg/kg doxorubicin (8 wild-type and 11 caspase-3-KO mice were used in the control noninjected groups). A Wilcoxon test of equality over strata (life-test procedure) was used to assess the significance of the observed difference.

malities (see Table S1 in the supplemental material). Expression of RasGAP, caspase-3, Akt, and actin was similar in given tissues and cells derived from wild-type and KI mice (Fig. 4F). The transmission of the mutated alleles occurred with normal Mendelian ratios (among 317 offspring obtained from breeding heterozygote +/D455A mice, 22.4% were +/+, 54.3% were +/D455A, and 23.7% were D455A/D455A).

As expected, fibroblasts derived from KI embryos were unable to cleave RasGAP in response to various apoptotic stimuli (Fig. 5A) and were more prone to apoptosis in response to these stimuli than control MEFs (Fig. 5B). Additionally, in contrast to what was observed with wild-type embryos, cells from KI embryos did not survive long-term trypsin digestion (Fig. 5C). MEFs from KI embryos were also impaired in their capacity to activate Akt in response to stress (Fig. 5D). The increased susceptibility of KI cells to death in response to stresses is consistent with the known ability of fragment N to stimulate Akt and inhibit apoptosis in cultured cell lines (47, 49, 50).

Mice that cannot cleave RasGAP at position 455 are unable to activate Akt in response to stress, and they experience increased apoptosis, tissue damage, and organ dysfunction. The KI mice were then used to assess the importance of RasGAP cleavage in Akt activation and in the protection of tissues and organs upon exposure to the pathophysiological challenges described for Fig. 1. In response to low UV-B exposure (0.05 J/cm^2), Akt was activated in about 10% of keratinocytes of wild-type mice (Fig. 6A). Akt activation was, however, not observed when the skin was exposed to higher UV-B doses (0.3 J/cm^2) (Fig. 6A) that led to strong caspase-3 activation (Fig. 6B). It is known that low caspase-3 activity leads to fragment N generation, while high caspase-3 activity induces fragment N cleavage into fragments that are no longer able to activate Akt (48). In skin samples, all the RasGAP antibodies that we have tested lit up bands in the 35- to 55-kDa range, precluding visualization of fragment N (52 kDa) (Fig. 6C). These bands may be nonspecifically recognized by the RasGAP antibodies, but it is more likely that they correspond to RasGAP degradation products that are generated in keratinocytes en route to their final differentiation stage in the cornified layer, a process that is known to be associated with massive activation of epidermal proteases (8). Fragment N2, one of the caspase-3-generated products of fragment N (49), was, however, seen in samples derived from skin exposed to 0.3 J/cm^2 UV-B but not in samples derived from skin exposed to 0.05 J/cm^2 UV-B (Fig. 6C). These results indicate that Akt is not activated under conditions where fragment N2 is produced, i.e., when fragment N is degraded. In contrast to what was observed in wild-type skin, low doses of UV-B only marginally

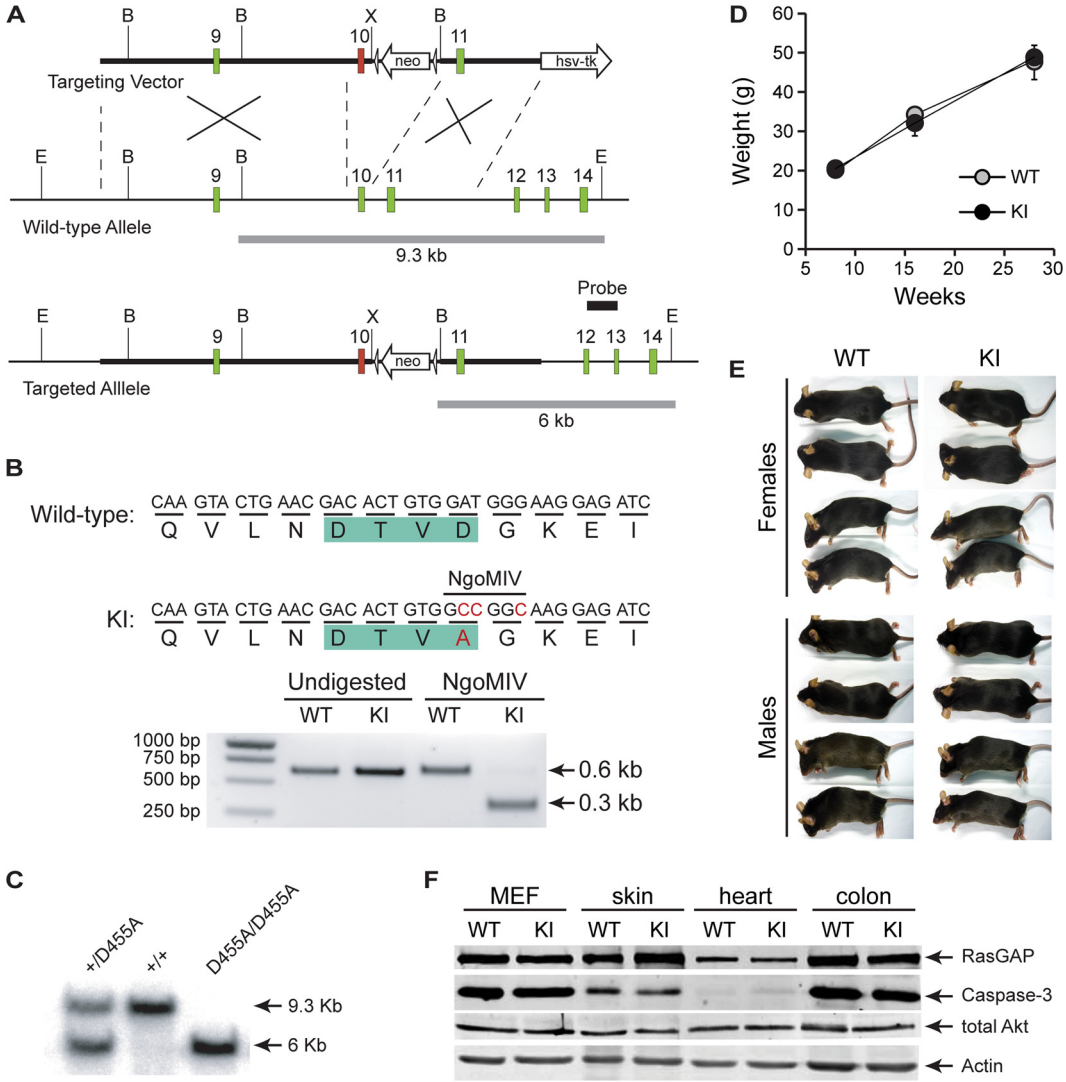

FIG 4 Generation of RasGAP$^{D455A/D455A}$ knock-in mice. (A) The targeting vector consists of mouse RasGAP exons 9, 10, and 11. Exon 10 (indicated in red) bears the RasGAP D455A mutation. E, X, and B, EcoRV, XhoI, and BamHI, respectively; gray bars below the alleles, length of the BamHI/EcoRV fragments recognized by the probe (black bar) when genotyping by Southern blot is performed. (B) Detection of the D455A allele by PCR. The D455A allele bears a new NgoMIV restriction site encompassing the aspartate-to-alanine mutation (in red) within the caspase recognition site in RasGAP (in green). Genomic DNA was subjected to PCR amplification using primers flanking exon 10. The amplified fragments, after digestion with NgoMIV or not, were separated on a 1.5% agarose gel. The presence of the D455A mutation results in cleavage of the ~600-bp PCR fragment into two comigrating ~300-bp fragments. (C) Tail-purified genomic DNA was digested with EcoRV and BamHI and tested by Southern blotting using the probe shown in panel A. (D) The body weight of wild-type and RasGAP$^{D455A/D455A}$ knock-in males was monitored at the indicated time points. Results correspond to the mean ± 95% CI of at least 9 determinations per condition. (E) Images from anesthetized 10-week-old mice. (F) The expression of RasGAP, caspase-3, Akt, and actin in the indicated cell type and tissues was assessed by Western blotting.

and nonsignificantly activated Akt in keratinocytes from KI skin (Fig. 6A). This correlated with increased numbers of cells expressing active caspase-3 (Fig. 6B) and cells undergoing apoptosis (Fig. 6D). When the skin was exposed to higher UV-B doses (0.3 J/cm^2), the extent of apoptosis in the skin of wild-type and KI mice was not significantly different, although there was a trend of a stronger apoptotic response in KI mice (Fig. 6D) that correlated with a tendency of KI mice to activate less Akt (compare the last two bars in Fig. 6A) but more caspase-3 (Fig. 6B) at high UV-B doses. Sunburn cells (see the example in Fig. 6E) were significantly augmented in the epidermis of 0.05-J/cm^2 UV-B-exposed KI skin compared to wild-type skin (Fig. 6E). The observed difference at higher UV-B doses (0.3 J/cm^2) was, however, not statistically significant.

Doxorubicin induced the cleavage of RasGAP into fragment N in the heart of wild-type mice (Fig. 7A). As expected, this was not observed in KI mice (Fig. 7A). Following doxorubicin injection, the number of cardiomyocytes with activated Akt did not increase in KI mice (Fig. 7B). This was also associated with an increase in the number of apoptotic cells in the heart (Fig. 7C). In response to doxorubicin, KI mice had more impaired cardiac function as measured by hemodynamic parameters (see Table S2 in the supplemental material). Specifically, end-systolic elastance, which is derived from end-systolic pressure volume curves (Fig. 7D) and which is a direct (load-independent) measure of the heart contractile activity, was significantly decreased in KI mice treated with doxorubicin (Fig. 7D and E).

Finally, enterocytes from KI mice were also affected in their

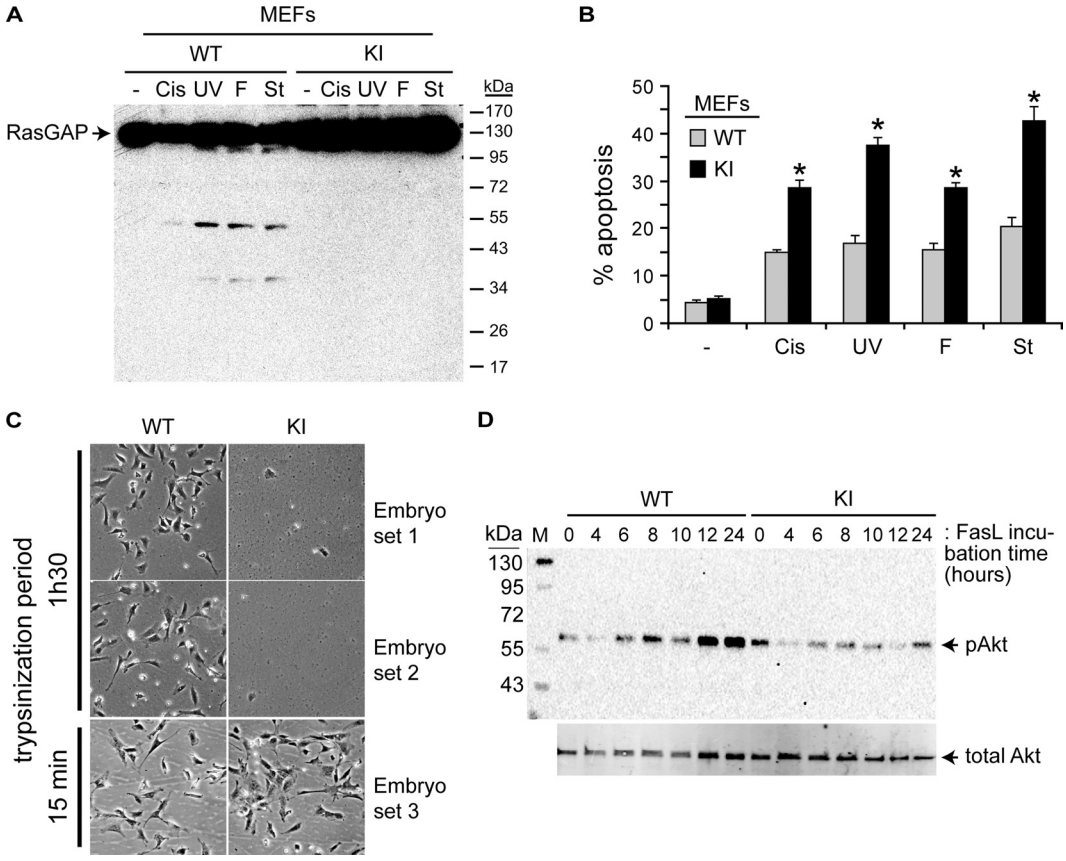

FIG 5 MEFs from RasGAP$^{D455A/D455A}$ knock-in mice do not cleave RasGAP and are more sensitive to apoptosis. (A and B) Wild-type (WT) and KI MEFs were left untreated (−) or treated with 15 μM cisplatin (Cis), 96 J/m^2 UV-C (UV), 15 ng/ml FasL (F), and 15 nM staurosporine (St). (A) Cells were lysed 24 h later and analyzed by Western blotting for the presence of RasGAP and its fragments using an anti-RasGAP polyclonal antibody. (B) Alternatively, apoptosis was scored. Results correspond to the mean ± 95% CI of 3 independent experiments ($n = 3$). (C) Mouse embryonic cells 1 day after their isolation using a trypsinization period of 1 h 30 min or 15 min (see Materials and Methods for details). (D) Wild-type and KI MEFs were treated with 5 ng/ml FasL for the indicated periods of time. Cells were then washed twice with PBS and then incubated for an additional hour in Dulbecco modified Eagle medium at 37°C before lysis. Akt activation and total Akt expression were assessed by Western blotting. Lane M, molecular mass markers.

capacity to activate Akt in response to DSS (Fig. 8A), and this was accompanied by an increased apoptotic response compared to what was seen in wild-type mice (Fig. 8B). At the clinical level, DSS-induced colon damage was more pronounced, as assessed by colon shortening (Fig. 8C) and a more severe DSS-mediated colitis development in KI mice than wild-type mice (Fig. 8D).

DISCUSSION

The role of caspase-3 in the induction of the antiapoptotic Akt kinase was investigated in adult caspase-3-knockout mice in relation to three different pathophysiological conditions: UV-B skin exposure, doxorubicin-induced cardiomyopathy, and DSS-mediated colitis. Each of these stresses led to Akt activation in the tissues affected by the stress. This was, however, blocked or strongly compromised in mice lacking caspase-3. This impaired Akt activation correlated with augmented cell death, tissue damage, and even lethality. A similar defect in Akt activation was observed in KI mice that expressed a caspase-3-resistant form of p120 RasGAP, and this was accompanied by increased apoptosis and stronger adverse effects: increased number of sunburn cells in UV-B-exposed skin, decreased heart function upon doxorubicin injection, and stronger DSS-mediated colitis development. This study therefore identifies a physiological protective mechanism against stress that relies on the activity of an executioner caspase.

Caspase-3 is now known to mediate many nonapoptotic functions in cells (15, 23, 24). It is involved in B cell homeostasis by negatively regulating B cell proliferation following antigen stimulation (46). Caspase-3 is also activated during T cell stimulation (32), and this may participate in T cell proliferation (2, 22). Additionally, caspase-3 is required for erythropoiesis (9). There is thus evidence that caspase-3 plays important functional roles in nondying hematopoietic cells, but it remains unclear how these cells counteract the apoptotic potential of caspase-3. Cleavage of RasGAP could have been one of the mechanisms allowing these cells to survive following caspase-3 activation. However, T and B cell development occurs normally in the D455A RasGAP KI mice (see Table S1 in the supplemental material). Similarly, the development of mature myeloid and erythroid lineage cells in the bone marrow proceeds normally in the KI mice (see Table S1 in the supplemental material). Therefore, hematopoietic cells use protective mechanisms other than those activated by the cleavage of RasGAP to inhibit apoptosis if caspase-3 is activated during their development.

Caspase-3 is necessary for the development of several tissues.

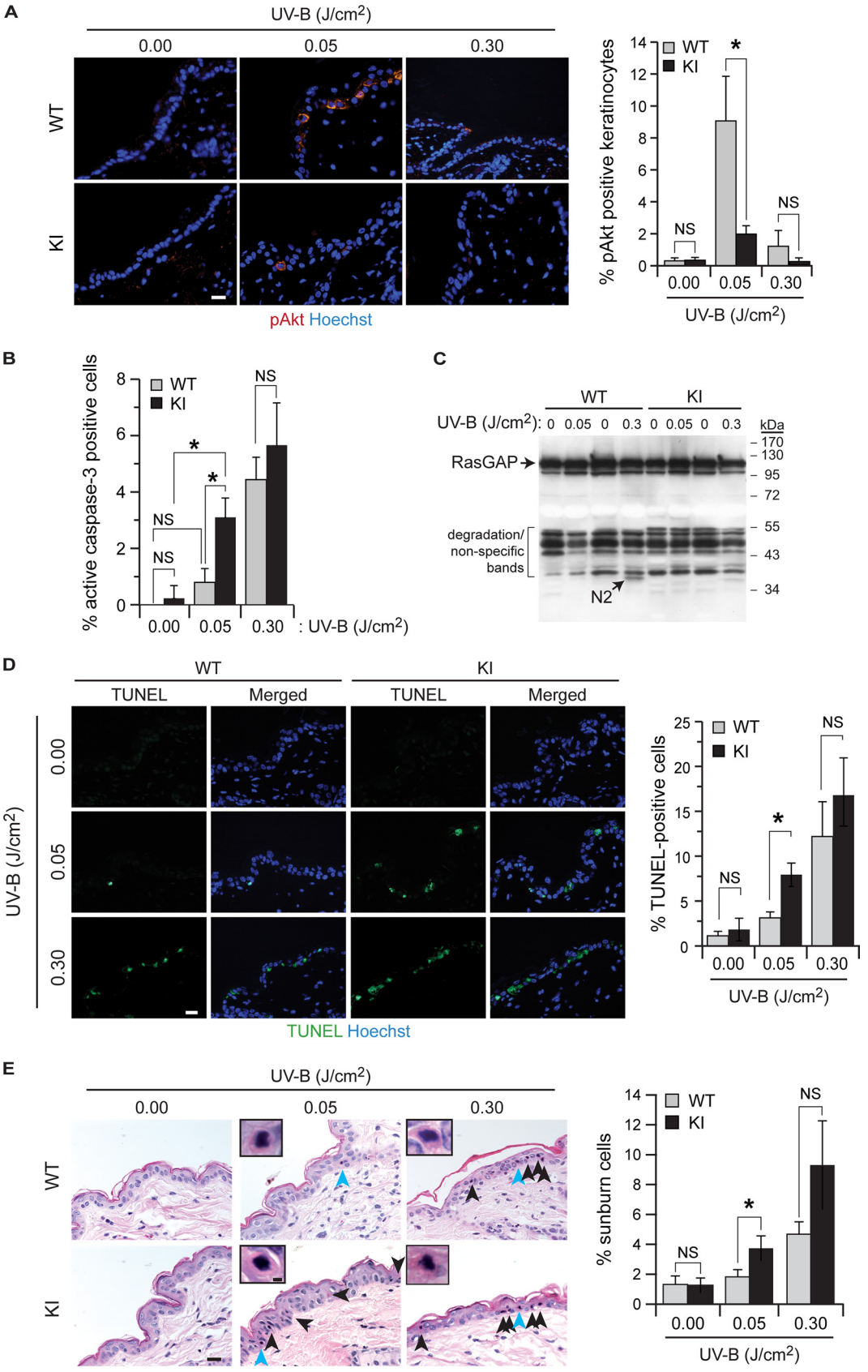

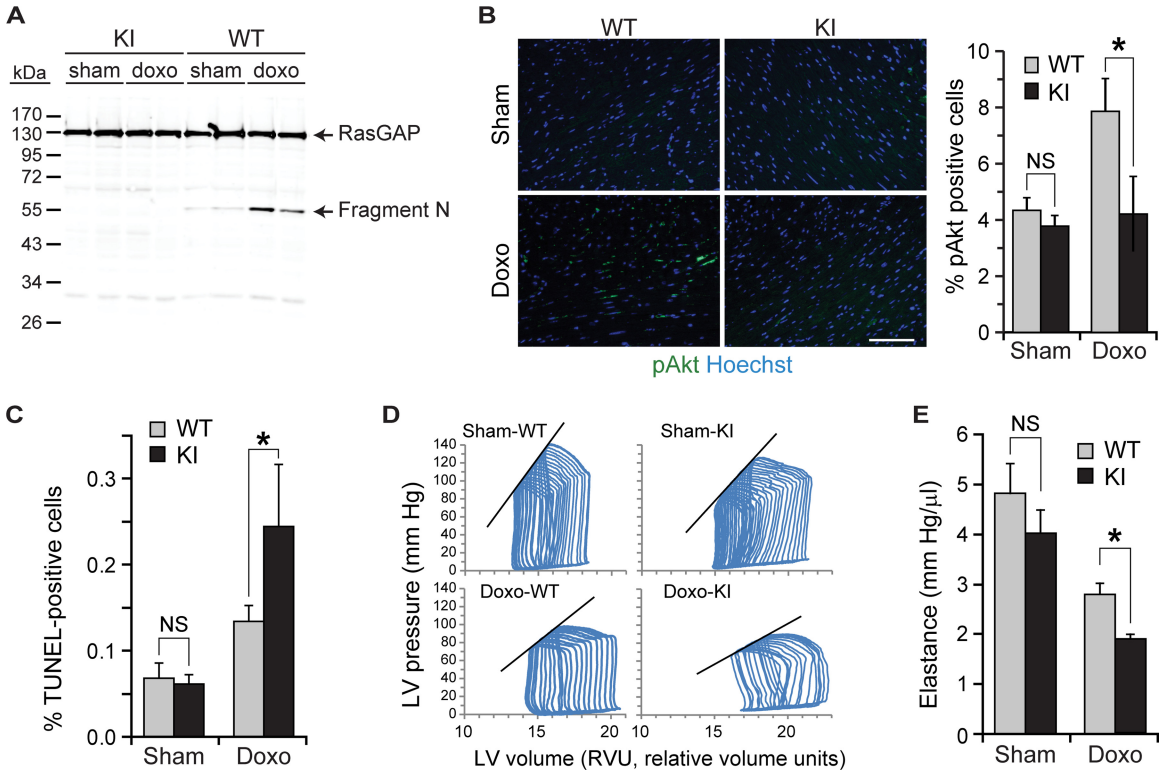

FIG 7 Role of RasGAP cleavage in heart of doxorubicin-treated mice. Wild-type (WT) and RasGAP$^{D455A/D455A}$ (KI) mice were injected with doxorubicin and analyzed 5 days later. (A) Western blot analysis of RasGAP cleavage. This experiment has been repeated once with similar results. (B) Histoimmunofluorescence detection and quantitation of active Akt. Bar, 100 μm. (C) Assessment of apoptosis by the TUNEL assay. (B and C) Results correspond to the mean ± 95% CI of measurements performed on 3 animals per condition (three independent experiments). (D) Representative examples of end-systolic left ventricular pressure-volume loops. (E) Heart contractility assessed by end-systolic elastance. Results correspond to the mean ± 95% CI of measurements performed on 9 to 11 animals per condition (three independent experiments).

Muscle development and osteoblast differentiation are compromised in the absence of caspase-3 (17, 33, 34). Caspase-3 also plays important functions in neurogenesis, synaptic activity, neuronal growth cone guidance, and glial development (7, 16, 37). Histological analyses of muscle, bone, and brain tissues did not reveal any defect in the KI mice (data now shown). Moreover, the growth curve and size of wild-type and KI mice were comparable (Fig. 4D and E). Hence, the mechanisms allowing tissues and organs to withstand caspase-3 activation during development do not rely on RasGAP cleavage and remain to be characterized.

In vitro data provided evidence that low caspase-3 activity induced by mild stress generates fragment N, which was responsible for Akt activation and promotion of cell survival. At higher caspase-3 activity induced by stronger insults, fragment N is further processed into fragments that can no longer stimulate Akt, and this favors apoptosis (47). The data obtained *in vivo* in UV-B-exposed skin are consistent with this model. Low doses of UV-B induced no further cleavage of fragment N (i.e., no production of fragment N2) in keratinocytes, and this was accompanied by Akt activation and absence of an apoptotic response. In contrast, high UV-B doses generated fragment N2 and Akt was no longer activated, and this led to keratinocyte cell death (Fig. 6). *In vivo*, therefore, RasGAP also functions as a caspase-3 activity sensor to determine whether cells within tissues and organs should be spared or die.

The levels of caspase-3 activation that are required to induce partial cleavage of RasGAP into fragment N are at least an order of magnitude lower than those necessary to induce apoptosis (48). *In vitro*, these low caspase activity levels are not easily detected (47). In response to the stress stimuli used in the present study that led to Akt activation, we could not visualize low caspase-3 activation by Western blotting in any of the tissues investigated, although in response to stronger stresses that did not lead to Akt activation (e.g., 0.3 J/cm^2 of UV-B [Fig. 6]), caspase-3 activation could be evidenced (Fig. 2A and B). Nonetheless, blocking caspases with chemical inhibitors or using mice lacking caspase-3 prevented Akt

FIG 6 Role of RasGAP cleavage in UV-B exposed skin. Skin of wild-type (WT) and RasGAP$^{D455A/D455A}$ (KI) mice was exposed to the indicated doses of UV-B. Mice were sacrificed 24 h later, and the exposed skin was isolated for biochemical and histological analyses. (A and B) Histoimmunofluorescence detection and quantitation of active Akt (A) and active caspase-3 (B). Results correspond to the mean ± 95% CI of measurements performed on 4 to 6 animals (three independent experiments). (C) Western blot analysis of RasGAP cleavage (the blot shown is representative of three independent experiments). (D) Assessment of apoptosis by the TUNEL assay. Results correspond to the mean ± 95% CI of measurements performed on 5 to 9 animals (three independent experiments). (E) Histological assessment of sunburn cells in the epidermis. Results correspond to the mean ± 95% CI of measurements performed on 9 to 11 animals (three independent experiments). Cells indicated by light blue arrowheads are enlarged in the insets. Bar, 20 μm.

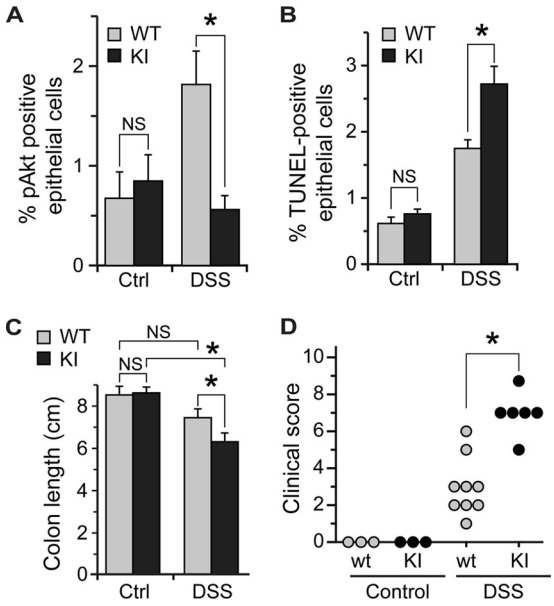

FIG 8 Role of RasGAP cleavage in colon of DSS-treated mice. Wild-type (WT) and RasGAP$^{D455A/D455A}$ (KI) mice were given DSS-containing water for 3 days and normal drinking water for four additional days. The mice were then sacrificed. (A) Quantitation of active Akt on histological sections. Results correspond to the mean ± 95% CI of measurements performed on 3 to 4 animals per condition (three independent experiments). (B) Assessment of apoptosis by the TUNEL assay. Results correspond to the mean ± 95% CI of measurements performed on 3 control and 6 to 7 DSS-treated animals per genotype (three independent experiments). (C) Colon damage assessed by variations in colon length. Results correspond to the mean ± 95% CI of measurements performed on 3 control and 7 to 9 DSS-treated animals per genotype (three independent experiments). (D) Clinical scoring of colitis performed on 7 to 10 animals per condition (three independent experiments). The data were analyzed with a Wilcoxon two-sample two-sided test.

activation induced by low stresses (Fig. 1 and 2). Therefore, caspase-3 exerts an important protective function in tissues and organs in a RasGAP cleavage-dependent manner under conditions where caspase-3 activation may be below the detection threshold of current caspase-3 activation assessment methods.

In conclusion, our study provides the first genetic evidence that in response to various pathology-inducing stresses caspase-3 itself activates the antiapoptotic Akt kinase and that this protective response is mediated through the cleavage of a given caspase-3 substrate, the ubiquitous p120 RasGAP protein. This defense mechanism allows an organism to dampen damage to tissues and organs induced by diverse pathogenic conditions. Hence, procedures aimed at activating the signaling pathways modulated by RasGAP cleavage may represent an attractive strategy to increase the resistance of individuals exposed to environmental or chemical stresses. Additionally, our work has direct implications for therapeutic protocols using caspase inhibitors, as inhibition of caspases could lead to unanticipated adverse effects by decreasing the ability of an organism to cleave RasGAP and defend itself.

ACKNOWLEDGMENTS

This work was supported by Swiss National Science Foundation grants 31003A_119876 and 31003A_141242 1/1 (to C.W.), 310030_135394/1 (to L.L.), and 310030_122012 (to W.H.) and by an Interdisciplinary Research Project subsidiary from the Faculty of Biology and Medicine, University of Lausanne, Lausanne, Switzerland (to C.W. and P.B.).

We thank Andrew Dwyer for critical reading of the manuscript. We thank the Transgenic Animal Facility of the Faculty of Biology and Medicine and the University Hospital (University of Lausanne) for generation of the knock-in mice.

H.K., N.P., and C.W. conceived the study. N.P. performed immunofluorescence experiments. H.K. and N.P. performed histology, TUNEL experiments, and the associated quantitation. J.W. generated the KI mice. J.-Y.Y., G.D., N.P., and C.W. performed the experiments on MEFs *in vitro*. N.G. and W.H. analyzed hematopoiesis and lymphopoiesis in mice. N.P. and P.B. performed the UV-B illumination experiments. H.K. and B.M. performed the DSS experiments. H.K. and L.L. analyzed cardiac functions in mice. C.W. wrote the paper. All authors discussed the results.

We declare that we have no conflict of interest.

REFERENCES

1. **Abraham MC, Shaham S.** 2004. Death without caspases, caspases without death. Trends Cell Biol. **14**:184–193.
2. **Alam A, Cohen LY, Aouad S, Sekaly RP.** 1999. Early activation of caspases during T lymphocyte stimulation results in selective substrate cleavage in nonapoptotic cells. J. Exp. Med. **190**:1879–1890.
3. **Bonnet MC, et al.** 2011. The adaptor protein FADD protects epidermal keratinocytes from necroptosis in vivo and prevents skin inflammation. Immunity **35**:572–582.
4. **Bulat N, et al.** 2011. RasGAP-derived fragment N increases the resistance of beta cells towards apoptosis in NOD mice and delays the progression from mild to overt diabetes. PLoS One **6**:e22609. doi:10.1371/journal.pone.0022609.
5. **Bulat N, Waeber G, Widmann C.** 2009. LDLs stimulate p38 MAPKs and wound healing through SR-BI independently of Ras and PI3 kinase. J. Lipid Res. **50**:81–89.
6. **Burguillos MA, et al.** 2011. Caspase signalling controls microglia activation and neurotoxicity. Nature **472**:319–324.
7. **Campbell DS, Holt CE.** 2003. Apoptotic pathway and MAPKs differentially regulate chemotropic responses of retinal growth cones. Neuron **37**:939–952.
8. **Candi E, Schmidt R, Melino G.** 2005. The cornified envelope: a model of cell death in the skin. Nat. Rev. Mol. Cell Biol. **6**:328–340.
9. **Carlile GW, Smith DH, Wiedmann M.** 2004. Caspase-3 has a nonapoptotic function in erythroid maturation. Blood **103**:4310–4316.
10. **Caserta TM, Smith AN, Gultice AD, Reedy MA, Brown TL.** 2003. Q-VD-OPh, a broad spectrum caspase inhibitor with potent antiapoptotic properties. Apoptosis **8**:345–352.
11. **Cuvillier O, et al.** 2001. Sphingosine generation, cytochrome c release, and activation of caspase-7 in doxorubicin-induced apoptosis of MCF7 breast adenocarcinoma cells. Cell Death Differ. **8**:162–171.
12. **Daniels F, Jr, Brophy D, Lobitz WC, Jr.** 1961. Histochemical responses of human skin following ultraviolet irradiation. J. Invest. Dermatol. **37**:351–357.
13. **Droin N, et al.** 2008. A role for caspases in the differentiation of erythroid cells and macrophages. Biochimie **90**:416–422.
14. **Eymin B, et al.** 1999. Caspase-induced proteolysis of the cyclin-dependent kinase inhibitor p27Kip1 mediates its anti-apoptotic activity. Oncogene **18**:4839–4847.
15. **Feinstein-Rotkopf Y, Arama E.** 2009. Can't live without them, can live with them: roles of caspases during vital cellular processes. Apoptosis **14**:980–995.
16. **Fernando P, Brunette S, Megeney LA.** 2005. Neural stem cell differentiation is dependent upon endogenous caspase 3 activity. FASEB J. **19**:1671–1673.
17. **Fernando P, Kelly JF, Balazsi K, Slack RS, Megeney LA.** 2002. Caspase 3 activity is required for skeletal muscle differentiation. Proc. Natl. Acad. Sci. U. S. A. **99**:11025–11030.
18. **Fujita J, et al.** 2008. Caspase activity mediates the differentiation of embryonic stem cells. Cell Stem Cell **2**:595–601.
19. **Giaime E, et al.** 2006. Caspase-3-derived C-terminal product of synphilin-1 displays antiapoptotic function via modulation of the p53-dependent cell death pathway. J. Biol. Chem. **281**:11515–11522.
20. **Holler N, et al.** 2003. Two adjacent trimeric Fas ligands are required for Fas signaling and formation of a death-inducing signaling complex. Mol. Cell. Biol. **23**:1428–1440.
21. **Jianhui L, et al.** 2010. Endotoxin impairs cardiac hemodynamics by

affecting loading conditions but not by reducing cardiac inotropism. Am. J. Physiol. Heart Circ. Physiol. **299**:H492–H501.
22. **Kennedy NJ, Kataoka T, Tschopp J, Budd RC.** 1999. Caspase activation is required for T cell proliferation. J. Exp. Med. **190**:1891–1896.
23. **Kuranaga E, Miura M.** 2007. Nonapoptotic functions of caspases: caspases as regulatory molecules for immunity and cell-fate determination. Trends Cell Biol. **17**:135–144.
24. **Launay S, et al.** 2005. Vital functions for lethal caspases. Oncogene **24**: 5137–5148.
25. **Leonard JR, Klocke BJ, D'Sa C, Flavell RA, Roth KA.** 2002. Strain-dependent neurodevelopmental abnormalities in caspase-3-deficient mice. J. Neuropathol. Exp. Neurol. **61**:673–677.
26. **Li Z, et al.** 2010. Caspase-3 activation via mitochondria is required for long-term depression and AMPA receptor internalization. Cell **141**:859–871.
27. **Liadis N, et al.** 2005. Caspase-3-dependent β-cell apoptosis in the initiation of autoimmune diabetes mellitus. Mol. Cell. Biol. **25**:3620–3629.
28. **Luciano F, Herrant M, Jacquel A, Ricci JE, Auberger P.** 2003. The p54 cleaved form of the tyrosine kinase Lyn generated by caspases during BCR-induced cell death in B lymphoma acts as a negative regulator of apoptosis. FASEB J. **17**:711–713.
29. **Mansilla S, Priebe W, Portugal J.** 2006. Mitotic catastrophe results in cell death by caspase-dependent and caspase-independent mechanisms. Cell Cycle **5**:53–60.
30. **McLaughlin B, et al.** 2003. Caspase 3 activation is essential for neuroprotection in preconditioning. Proc. Natl. Acad. Sci. U. S. A. **100**:715–720.
31. **Michod D, Widmann C.** 2007. TAT-RasGAP$_{317-326}$ requires p53 and PUMA to sensitize tumor cells to genotoxins. Mol. Cancer Res. **5**:497–507.
32. **Miossec C, Dutilleul V, Fassy F, Diu-Hercend A.** 1997. Evidence for CPP32 activation in the absence of apoptosis during T lymphocyte stimulation. J. Biol. Chem. **272**:13459–13462.
33. **Miura M, et al.** 2004. A crucial role of caspase-3 in osteogenic differentiation of bone marrow stromal stem cells. J. Clin. Invest. **114**:1704–1713.
34. **Mogi M, Togari A.** 2003. Activation of caspases is required for osteoblastic differentiation. J. Biol. Chem. **278**:47477–47482.
35. **Newton K, Strasser A.** 2003. Caspases signal not only apoptosis but also antigen-induced activation in cells of the immune system. Genes Dev. **17**:819–825.
36. **Ohkawara T, et al.** 2005. Transgenic over-expression of macrophage migration inhibitory factor renders mice markedly more susceptible to experimental colitis. Clin. Exp. Immunol. **140**:241–248.
37. **Oomman S, Strahlendorf H, Dertien J, Strahlendorf J.** 2006. Bergmann glia utilize active caspase-3 for differentiation. Brain Res. **1078**:19–34.
38. **Pacher P, et al.** 2003. Potent metalloporphyrin peroxynitrite decomposition catalyst protects against the development of doxorubicin-induced cardiac dysfunction. Circulation **107**:896–904.
39. **Pacher P, et al.** 2004. Left ventricular pressure-volume relationship in a rat model of advanced aging-associated heart failure. Am. J. Physiol. Heart Circ. Physiol. **287**:H2132–H2137.
40. **Parcellier A, Tintignac LA, Zhuravleva E, Hemmings BA.** 2008. PKB and the mitochondria: AKTing on apoptosis. Cell. Signal. **20**:21–30.
41. **Peter ME.** 2011. Programmed cell death: apoptosis meets necrosis. Nature **471**:310–312.
42. **Rincheval V, Renaud F, Lemaire C, Mignotte B, Vayssiere JL.** 1999. Inhibition of Bcl-2-dependent cell survival by a caspase inhibitor: a possible new pathway for Bcl-2 to regulate cell death. FEBS Lett. **460**:203–206.
43. **Slee EA, Adrain C, Martin SJ.** 2001. Executioner caspase-3, -6, and -7 perform distinct, non-redundant roles during the demolition phase of apoptosis. J. Biol. Chem. **276**:7320–7326.
44. **Sordet O, et al.** 2002. Specific involvement of caspases in the differentiation of monocytes into macrophages. Blood **100**:4446–4453.
45. **Taylor RC, Cullen SP, Martin SJ.** 2008. Apoptosis: controlled demolition at the cellular level. Nat. Rev. Mol. Cell Biol. **9**:231–241.
46. **Woo M, et al.** 2003. Caspase-3 regulates cell cycle in B cells: a consequence of substrate specificity. Nat. Immunol. **4**:1016–1022.
47. **Yang J-Y, et al.** 2004. Partial cleavage of RasGAP by caspases is required for cell survival in mild stress conditions. Mol. Cell. Biol. **24**:10425–10436.
48. **Yang J-Y, Walicki J, Michod D, Dubuis G, Widmann C.** 2005. Impaired Akt activity down-modulation, caspase-3 activation, and apoptosis in cells expressing a caspase-resistant mutant of RasGAP at position 157. Mol. Biol. Cell **16**:3511–3520.
49. **Yang J-Y, Widmann C.** 2001. Antiapoptotic signaling generated by caspase-induced cleavage of RasGAP. Mol. Cell. Biol. **21**:5346–5358.
50. **Yang J-Y, Widmann C.** 2002. The RasGAP N-terminal fragment generated by caspase cleavage protects cells in a Ras/PI3K/Akt-dependent manner that does not rely on NFκB activation. J. Biol. Chem. **277**:14641–14646.
51. **Youn HJ, et al.** 2005. Induction of caspase-independent apoptosis in H9c2 cardiomyocytes by adriamycin treatment. Mol. Cell. Biochem. **270**: 13–19.